

Is GRB 050904 a super-long burst?

Y. C. Zou, Z. G. Dai and D. Xu ¹

ABSTRACT

By considering synchrotron radiative process in the internal shock model and assuming that all internal shocks are nearly equally energetic, we analyze the gamma-ray burst (GRB) emission at different radii corresponding to different observed times. We apply this model to GRB 050904 and find that our analytical results can provide a natural explanation for the multi-band observations of GRB 050904. This suggests that the X-ray flare emission and the optical emission of this burst could have originated from internal shocks being due to collisions among nearly-equally-energetic shells ejected from the central engine. Thus GRB 050904 appears to be a burst with super-long central engine activity.

Subject headings: gamma rays: bursts - hydrodynamics - relativity - shock waves

1. Introduction

The gamma-ray burst (GRB) 050904 was an explosive event at redshift of $z = 6.29 \pm 0.01$, which has been measured through various methods (Kawai et al. 2005; Price et al. 2005; Haislip et al. 2005). After the Swift trigger (Cummings et al. 2005), multi-wavelength observations of this high-redshift burst were performed. The γ -ray isotropic-equivalent energy of this burst $E_{\gamma,iso}$ was between 6.6×10^{53} ergs and 3.2×10^{54} ergs (Cusumano et al. 2005). Boër et al. (2005) observed the optical emission at times of 86 s to 1666 s. The optical afterglow and its spectrum were analyzed quickly (Haislip et al. 2005; Tagliaferri et al. 2005). A break of the optical afterglow light curve was also observed at about 2.6 ± 1.0 days (Tagliaferri et al. 2005). The optical emission appears to be understood in either both the late internal shock model or the reverse-forward shock model (Wei et al. 2005).

One of the most remarkable features of this burst is a long lasting variability of the X-ray emission, showing several X-ray flares (XRFs). Watson et al. (2005) and Cusumano et al.

¹Department of Astronomy, Nanjing University, Nanjing 210093, China; zouyc@nju.edu.cn, dzg@nju.edu.cn.

(2005) suggested that this variability may be due to a long-lasting activity of the central engine. The XRFs were also found in some other GRBs (Nousek et al. 2006; O’Brien et al. 2006). Burrows et al. (2005), Fan & Wei (2005), Zhang et al. (2005) and Wu et al. (2005) assumed late central engine activities to interpret the XRFs. The plausible origin models of XRFs were recently proposed, e.g., the magnetic activity of a newborn millisecond pulsar (Dai et al. 2006), fragmentation of a neutron star by a black hole in a compact object binary (Faber et al. 2006), fragmentation of an accretion disk (Perna et al. 2006), and magnetic barrier-driven modulation of an accretion disk (Proga et al. 2006). However, there has not yet been any explicit and detailed investigation on this highly-variable light curve. Enlightened by the internal shock model to interpret the γ -ray emission (Rees & Mészáros 1994) and prompt optical emission (Mészáros & Rees 1999), we assume that all the highly-variable X-ray emission (even at very late times) originate from internal shocks. These shocks occur when many faster shells with equal energy and equal mass catch up with a slower shell with much more kinetic energy and mass. By fitting the peaks of the X-ray and optical light curves, we find that these internal shocks can lead to the observed X-ray and optical emission. We describe an internal-shock model in §2, fit the peaks of X-ray and optical light curves of GRB 050904 in §3. We summarize our results in §4.

2. Model

We assume two cold shells labeled with 1 and 4, whose isotropic kinetic energies are E_1 and E_4 , widths are $\Delta_{1,0}$ and $\Delta_{4,0}$ in the cosmological rest frame, and Lorentz factors are γ_1 and γ_4 ($\gamma_4 \gg \gamma_1 \gg 1$), respectively. The shells come from the central engine with time lag T (also in the rest frame). Shell 4 catches up with shell 1 at radius $r_{\text{int}} \simeq 2\gamma_1^2 cT$ and then two internal shocks occur, that is, a forward shock that propagates into shell 1 and a reverse shock that propagates into shell 4. Four regions are divided by the reverse and forward shocks: unshocked shell 1 (region 1), shocked gas of shell 1 (region 2), shocked gas of shell 4 (region 3) and unshocked shell 4 (region 4), with a contact discontinuity (CD) surface separating region 2 and region 3. Figure 1 gives a sketch of this model. The number densities of region 1 and region 4 at radius r are $n_1 = E_1/(4\pi r^2 \gamma_1^2 \Delta_{1,0} m_p c^2)$ and $n_4 = E_4/(4\pi r^2 \gamma_4^2 \Delta_{4,0} m_p c^2)$ respectively. To produce plenty of X-rays and γ -rays, it is required that the reverse-shocked materials are relativistic, i.e., $\gamma_{34} \simeq \frac{1}{\sqrt{2}} \left(\frac{\gamma_4}{\gamma_1}\right)^{1/2} f^{-1/4} \gg 1$ (Sari & Piran 1995; Wu, Dai & Huang 2003; Zou, Wu & Dai 2005), where γ_{34} is the relative Lorentz factor between regions 4 and 3, and the number density ratio is defined as $f \equiv n_4/n_1$.

To calculate the width of the coasting shell, we define the spreading radius $R_\Delta \equiv \gamma^2 \Delta_0$ (Mészáros & Rees 1993; Piran, Shemi & Narayan 1993). For the internal shocks of

our interests, if $r < \min(R_{\Delta,1} = 1.0 \times 10^{15} \gamma_{1,1.5}^2 \Delta_{1,0,12} \text{cm}, R_{\Delta,4} = 1.0 \times 10^{16} \gamma_{4,3}^2 \Delta_{4,0,10} \text{cm})$, the width of the shells can be considered to be constant, and for $r > \max(R_{\Delta,1}, R_{\Delta,4})$, the width should be regarded as r/γ_1^2 and r/γ_4^2 for the spreading of the shells. The conventional notation $Q_k = Q/10^k$ with cgs units is used in this paper except for special explanations. We now consider these two cases.

2.1. No-spreading case

At radius $r < \min(R_{\Delta,1}, R_{\Delta,4})$, for a certain set of parameters $\Delta_{1,0,12} = \Delta_{4,0,10} = E_{1,54} = E_{4,51} = \gamma_{1,1.5} = \gamma_{4,3} = 1$, one obtains $\gamma_{14}^2 f \simeq 2.5 \times 10^{-2} E_{1,54}^{-1} E_{4,51} \Delta_{1,0,12} \Delta_{4,0,10}^{-1} \ll 1$ (where γ_{14} is the relative Lorentz factor between regions 4 and 1), implying that the forward shock is Newtonian, and $\gamma_{14}^2/f \simeq 2.5 \times 10^6 E_{1,54} E_{4,51}^{-1} \Delta_{1,0,12}^{-1} \Delta_{4,0,10} \gamma_{1,1.5}^{-4} \gamma_{4,3}^4 \gg 1$, which shows that the reverse shock is relativistic. Using the shock conditions (Blandford & McKee 1976), and keeping equality of pressures and Lorentz factors of the materials at two sides of the contact discontinuity (Sari & Piran 1995), we can obtain the number densities n_2, n_3 , and energy densities e_2, e_3 of the shocked regions in the comoving frame,

$$n_2 \simeq 1.0 \times 10^{10} (1+z)^2 E_{1,54} \Delta_{1,0,12}^{-1} \gamma_{1,1.5}^{-6} t_{\oplus,2}^{-2} \text{cm}^{-3}, \quad (1)$$

$$n_3 \simeq 9.3 \times 10^6 (1+z)^2 E_{4,51} \Delta_{4,0,10}^{-1} \gamma_{1,1.5}^{-5} \gamma_{4,3}^{-1} t_{\oplus,2}^{-2} \text{cm}^{-3}, \quad (2)$$

$$e_2 = e_3 \simeq 2.2 \times 10^5 (1+z)^2 E_{4,51} \Delta_{4,0,10}^{-1} \gamma_{1,1.5}^{-6} t_{\oplus,2}^{-2} \text{erg cm}^{-3}. \quad (3)$$

The Lorentz factor $\gamma_2 = \gamma_3 \simeq \gamma_1 \simeq 31.6 \gamma_{1,1.5}$. Here t_{\oplus} is the observer's time.

Assuming that the reverse shock lasts from r_{int} to $r_{int} + \delta r$, we find $\delta r \simeq 1.0 \times 10^{13} \gamma_{1,1.5}^2 \Delta_{4,0,10} \text{cm}$, which corresponds to a pulse from the beginning to peak. In the observer's frame ($dt_{\oplus} = (1+z)dr/(2\gamma^2 c)$), this lasting time is

$$\delta t_{\oplus} \simeq 0.17(1+z) \Delta_{4,0,10} \text{ s}. \quad (4)$$

By considering the synchrotron emission at the reverse shock-crossing time, which corresponds to the peak emission time, we obtain the characteristic frequencies $\nu_{m,2,p}$ and $\nu_{m,3,p}$, cooling frequencies $\nu_{c,2,p}$ and $\nu_{c,3,p}$, synchrotron self-absorption frequencies $\nu_{a,2,p}$ and $\nu_{a,3,p}$, and the maximum flux densities $f_{\nu,\text{max},2,p}$ and $f_{\nu,\text{max},3,p}$ in the observer's frame (see Zou, Wu & Dai 2005, for original formulae of synchrotron emission)

$$\nu_{m,2,p} \simeq 1.3 \times 10^{11} E_{1,54}^{-2} E_{4,51}^{\frac{5}{2}} \Delta_{1,0,12}^2 \Delta_{4,0,10}^{-\frac{5}{2}} \epsilon_{B,-1}^{\frac{1}{2}} \epsilon_{e,-0.5}^2 \gamma_{1,1.5}^{-2} \zeta_{1/6}^2 t_{\oplus,2}^{-1} \text{Hz}, \quad (5)$$

$$\nu_{m,3,p} \simeq 1.5 \times 10^{17} E_{4,51}^{\frac{1}{2}} \Delta_{4,0,10}^{-\frac{1}{2}} \epsilon_{B,-1}^{\frac{1}{2}} \epsilon_{e,-0.5}^2 \gamma_{1,1.5}^{-4} \gamma_{4,3}^2 \zeta_{1/6}^2 t_{\oplus,2}^{-1} \text{Hz}, \quad (6)$$

$$\nu_{c,2,p} = \nu_{c,3,p} \simeq 1.2 \times 10^{15} (1+z)^{-4} E_{4,51}^{-\frac{3}{2}} \Delta_{4,0,10}^{-\frac{1}{2}} \epsilon_{B,-1}^{-\frac{3}{2}} \gamma_{1,1.5}^8 t_{\oplus,2}^3 \text{Hz}, \quad (7)$$

$$\nu_{a,2,p} \simeq 3.2 \times 10^{14} (1+z)^{-\frac{5}{18}} E_{1,54}^{-\frac{7}{36}} E_{4,51}^{\frac{5}{9}} \Delta_{1,0,12}^{\frac{7}{36}} \Delta_{4,0,10}^{-\frac{5}{9}} \epsilon_{B,-1}^{\frac{1}{12}} \epsilon_{e,-0.5}^{\frac{1}{3}} \gamma_{1,1.5}^{-\frac{8}{9}} \zeta_{1/6}^{\frac{1}{3}} t_{\oplus,2}^{-\frac{13}{18}} \text{Hz}, \quad (8)$$

$$\nu_{a,3,p} \simeq 1.2 \times 10^{14} (1+z)^{-\frac{1}{3}} E_{4,51}^{\frac{1}{3}} \Delta_{4,0,10}^{-\frac{1}{3}} \gamma_{1,1.5}^{-\frac{2}{3}} \gamma_{4,3}^{-\frac{1}{3}} t_{\oplus,2}^{-\frac{2}{3}} \text{Hz}, \quad (9)$$

$$f_{\nu,\text{max},2,p} \simeq 8.0 \times 10^2 D_{28}^{-2} E_{1,54}^{\frac{1}{2}} E_{4,51} (1+z)^2 \Delta_{1,0,12}^{-\frac{1}{2}} \epsilon_{B,-1}^{\frac{1}{2}} \gamma_{1,1.5}^{-2} t_{\oplus,2}^{-1} \text{Jy}, \quad (10)$$

$$f_{\nu,\text{max},3,p} \simeq 0.47 (1+z)^2 D_{28}^{-2} E_{4,51}^{\frac{3}{2}} \Delta_{4,0,10}^{-\frac{1}{2}} \epsilon_{B,-1}^{\frac{1}{2}} \gamma_{1,1.5}^{-2} \gamma_{4,3}^{-1} t_{\oplus,2}^{-1} \text{Jy}, \quad (11)$$

where $\zeta_{1/6} = 6(p-2)/(p-1)$, p is the spectral index of the shock-accelerated electrons, D is the luminosity distance from the burst to the observer (as a function of redshift z), and ϵ_e and ϵ_B are the fractions of the internal energy density that were carried by electrons and magnetic fields, respectively. In this paper, p is taken to be 2.2, and ϵ_e and ϵ_B are equal for both region 2 and region 3. Note that the expressions of $\nu_{a,2,p}$ and $\nu_{a,3,p}$ are only valid in the cases of $\nu_{c,2,p} < \nu_{m,2,p} < \nu_{a,2,p}$ and $\nu_{a,3,p} < \nu_{c,3,p} < \nu_{m,3,p}$.

From the above equations, we see $\nu_{c,2,p} < \nu_{m,2,p} < \nu_{a,2,p}$ and $\nu_{a,3,p} < \nu_{c,3,p} < \nu_{m,3,p}$ for typical parameters. The flux density in the fast-cooling case at the peak time is then given by

$$f_{\nu,2,p} \simeq$$

$$\begin{cases} 2.4 \times 10^8 (1+z)^{-1} D_{28}^{-2} E_{4,51}^{-1} \epsilon_{B,-1}^{-1} \gamma_{1,1.5}^8 \nu_{18}^2 t_{\oplus,2}^4 \text{Jy}, & \nu < \nu_{c,2,p} < \nu_{m,2,p} < \nu_{a,2,p}, \\ 7.1 \times 10^9 (1+z) D_{28}^{-2} E_{4,51}^{-\frac{1}{4}} \Delta_{4,0,10}^{\frac{1}{4}} \epsilon_{B,-1}^{-\frac{1}{4}} \gamma_{1,1.5}^4 \nu_{18}^{\frac{5}{2}} t_{\oplus,2}^{\frac{5}{2}} \text{Jy}, & \nu_{c,2,p} < \nu < \nu_{a,2,p}, \\ 2.0 \times 10^{-3} D_{28}^{-2} E_{1,54}^{-\frac{7}{10}} E_{4,51}^{\frac{7}{4}} \Delta_{1,0,12}^{\frac{7}{10}} \Delta_{4,0,10}^{-\frac{7}{4}} \epsilon_{B,-1}^{\frac{6}{20}} \epsilon_{e,-0.5}^{\frac{6}{5}} \gamma_{1,1.5}^{\frac{4}{5}} \nu_{18}^{-\frac{11}{10}} \zeta_{1/6}^{\frac{6}{5}} t_{\oplus,2}^{-\frac{1}{10}} \text{Jy}, & \nu_{c,2,p} < \nu_{m,2,p} < \nu_{a,2,p} < \nu. \end{cases} \quad (12)$$

for the forward shock emission, and

$$f_{\nu,3,p} \simeq$$

$$\begin{cases} 3.3 \times 10^8 (1+z)^{-1} D_{28}^{-2} E_{4,51}^{-1} \epsilon_{B,-1}^{-1} \gamma_{1,1.5}^8 \nu_{18}^2 t_{\oplus,2}^4 \text{Jy}, & \nu < \nu_{c,3,p} < \nu_{a,3,p} < \nu_{m,3,p}, \\ 9.6 \times 10^9 (1+z)^{\frac{10}{3}} D_{28}^{-2} E_{4,51}^{-\frac{1}{4}} \Delta_{4,0,10}^{\frac{1}{4}} \epsilon_{B,-1}^{-\frac{1}{4}} \gamma_{1,1.5}^4 \nu_{18}^{\frac{5}{2}} t_{\oplus,2}^{\frac{5}{2}} \text{Jy}, & \nu_{c,3,p} < \nu < \nu_{a,3,p} < \nu_{m,3,p}, \\ 1.6 \times 10^{-2} D_{28}^{-2} E_{4,51}^{\frac{3}{4}} \Delta_{4,0,10}^{-\frac{3}{4}} \epsilon_{B,-1}^{-\frac{1}{4}} \gamma_{1,1.5}^2 \gamma_{4,3}^{-1} \nu_{18}^{-\frac{1}{2}} t_{\oplus,2}^{\frac{1}{2}} \text{Jy}, & \nu_{c,3,p} < \nu_{a,3,p} < \nu < \nu_{m,3,p}, \\ 5.2 \times 10^{-3} D_{28}^{-2} E_{4,51}^{\frac{21}{20}} \Delta_{4,0,10}^{-\frac{21}{20}} \epsilon_{B,-1}^{\frac{1}{20}} \epsilon_{e,-0.5}^{\frac{6}{5}} \gamma_{1,1.5}^{-\frac{2}{5}} \gamma_{4,3}^{\frac{1}{5}} \zeta_{1/6}^{\frac{6}{5}} \nu_{18}^{-\frac{11}{10}} t_{\oplus,2}^{-\frac{1}{10}} \text{Jy}, & \nu_{c,3,p} < \nu_{a,3,p} < \nu_{m,3,p} < \nu, \end{cases} \quad (13)$$

for the reverse shock emission.

2.2. Spreading case

In the case of $r > \max(R_{\Delta,1}, R_{\Delta,4})$, the widths of the shells become $\Delta_1 \simeq r/\gamma_1^2$ and $\Delta_4 \simeq r/\gamma_4^2$ because of the spreading effect. For the same parameters as §2.1, $\gamma_{14}^2 f \simeq$

$0.5E_{1,54}^{-1}E_{4,51}\gamma_{1,1.5}^{-2}\gamma_{4,3}^2 < 1$, showing that the forward shock can be considered as Newtonian approximately, and $\gamma_{14}^2/f \simeq 2.5 \times 10^4 E_{1,54}E_{4,51}^{-1}\gamma_{1,1.5}^{-2}\gamma_{4,3}^2 \gg 1$, implying that the reverse shock is still relativistic.

Using the shock conditions as in §2.1, we obtain

$$n_2 \simeq 1.7 \times 10^9 (1+z)^3 E_{1,54} \gamma_{1,1.5}^{-6} t_{\oplus,2}^{-3} \text{ cm}^{-3}, \quad (14)$$

$$n_3 \simeq 1.5 \times 10^7 (1+z)^3 E_{4,51} \gamma_{1,1.5}^{-7} \gamma_{4,3} t_{\oplus,2}^{-3} \text{ cm}^{-3}, \quad (15)$$

$$e_2 = e_3 \simeq 3.7 \times 10^5 (1+z)^3 E_{4,51} \gamma_{1,1.5}^{-8} \gamma_{4,3}^2 t_{\oplus,2}^{-3} \text{ erg cm}^{-3}, \quad (16)$$

$$\gamma_2 = \gamma_3 \simeq \gamma_1 \simeq 31.6\gamma_{1,1.5}. \quad (17)$$

The distance for the reverse shock to cross shell 4 is $\delta r \simeq 6.0 \times 10^{12} (1+z)^{-1} \gamma_{4,3}^{-1} \gamma_{1,1.5}^2 t_{\oplus,2} \text{ cm}$, and the rising time of the pulse in the observer's frame is $\delta t_{\oplus} \simeq 0.2 \gamma_{4,3}^{-1} t_{\oplus,2} \text{ s}$.

The corresponding emission values at the peak time are given by

$$\nu_{m,2,p} \simeq 1.6 \times 10^{13} (1+z)^{\frac{1}{2}} E_{1,54}^{-2} E_{4,51}^{\frac{5}{2}} \epsilon_{B,-1}^{\frac{1}{2}} \epsilon_{e,-0.5}^2 \gamma_{1,1.5}^{-7} \gamma_{4,3}^5 \zeta_{1/6}^2 t_{\oplus,2}^{-\frac{3}{2}} \text{ Hz}, \quad (18)$$

$$\nu_{m,3,p} \simeq 2.0 \times 10^{17} (1+z)^{\frac{1}{2}} E_{4,51}^{\frac{1}{2}} \epsilon_{B,-1}^{\frac{1}{2}} \epsilon_{e,-0.5}^2 \gamma_{1,1.5}^{-\frac{5}{2}} \gamma_{4,3}^3 \zeta_{1/6}^2 t_{\oplus,2}^{-\frac{3}{2}} \text{ Hz}, \quad (19)$$

$$\nu_{c,2,p} = \nu_{c,3,p} \simeq 1.5 \times 10^{15} (1+z)^{-\frac{7}{2}} E_{4,51}^{-\frac{3}{2}} \epsilon_{B,-1}^{-\frac{3}{2}} \gamma_{1,1.5}^7 \gamma_{4,3}^5 t_{\oplus,2}^{\frac{5}{2}} \text{ Hz}, \quad (20)$$

$$\nu_{a,2,p} \simeq 6.4 \times 10^{14} (1+z)^{\frac{1}{12}} E_{1,54}^{-\frac{7}{12}} E_{4,51}^{\frac{5}{9}} \epsilon_{B,-1}^{\frac{1}{12}} \epsilon_{e,-0.5}^{\frac{1}{3}} \gamma_{1,1.5}^{-2} \gamma_{4,3}^{\frac{10}{9}} \zeta_{1/6}^{\frac{1}{3}} t_{\oplus,2}^{-\frac{13}{12}} \text{ Hz}, \quad (21)$$

$$\nu_{a,3,p} \simeq 2.0 \times 10^{13} (1+z)^{\frac{14}{5}} E_{4,51}^{\frac{9}{5}} \epsilon_{B,-1}^{\frac{6}{5}} \gamma_{1,1.5}^{-8} \gamma_{4,3}^{-\frac{1}{5}} t_{\oplus,2}^{-\frac{19}{5}} \text{ Hz}, \quad (22)$$

$$f_{\nu,\text{max},2,p} \simeq 0.033 (1+z)^{\frac{5}{2}} D_{28}^{-2} E_{1,54}^{\frac{1}{2}} E_{4,51} \epsilon_{B,-1}^{\frac{1}{2}} \gamma_{1,1.5}^{-2} t_{\oplus,2}^{-\frac{3}{2}} \text{ Jy}, \quad (23)$$

$$f_{\nu,\text{max},3,p} \simeq 0.6 (1+z)^{\frac{5}{2}} D_{28}^{-2} E_{4,51}^{\frac{3}{2}} \epsilon_{B,-1}^{\frac{1}{2}} \gamma_{1,1.5}^{-3} t_{\oplus,2}^{-\frac{3}{2}} \text{ Jy}. \quad (24)$$

Note that the expressions of $\nu_{a,2,p}$ and $\nu_{a,3,p}$ are valid only in the cases of $\nu_{m,2,p} < \nu_{c,2,p} < \nu_{a,2,p}$ and $\nu_{a,3,p} < \nu_{c,3,p} < \nu_{m,3,p}$ respectively.

In the case of $\nu_{m,2,p} < \nu_{c,2,p} < \nu_{a,2,p}$, the corresponding flux density of the forward shock emission is

$$f_{\nu,2,p} \simeq$$

$$\begin{cases} 2.1 \times 10^7 (1+z) D_{28}^{-2} E_{1,54}^{-1} E_{4,51} \epsilon_{e,-0.5} \gamma_{1,1.5} \gamma_{4,3}^2 \nu_{18}^2 \zeta_{1/6}^2 t_{\oplus,2}^2 \text{ Jy}, & \nu < \nu_{m,2,p} < \nu_{c,2,p} < \nu_{a,2,p}, \\ 5.2 \times 10^9 (1+z)^{\frac{3}{4}} D_{28}^{-2} E_{4,51}^{-\frac{1}{4}} \epsilon_{B,-1}^{-\frac{1}{4}} \gamma_{1,1.5}^{\frac{9}{2}} \gamma_{4,3}^{-\frac{1}{2}} \nu_{18}^{\frac{5}{2}} t_{\oplus,2}^{\frac{11}{4}} \text{ Jy}, & \nu_{m,2,p} < \nu < \nu_{a,2,p}, \\ 1.7 \times 10^{-2} (1+z)^{\frac{21}{20}} D_{28}^{-2} E_{1,54}^{-\frac{7}{10}} E_{4,51}^{\frac{7}{4}} \epsilon_{B,-1}^{\frac{1}{20}} \epsilon_{e,-0.5}^{\frac{6}{5}} \gamma_{1,1.5}^{-\frac{27}{10}} \gamma_{4,3}^{\frac{7}{2}} \nu_{18}^{-\frac{11}{10}} \zeta_{1/6}^{\frac{6}{5}} t_{\oplus,2}^{-\frac{23}{20}} \text{ Jy}, & \nu_{m,2,p} < \nu_{c,2,p} < \nu_{a,2,p} < \nu. \end{cases} \quad (25)$$

As the cooling frequency $\nu_{c,2,p}$ exceeds the self-absorption frequency $\nu_{a,2,p}$ at time $t_{\oplus} \simeq 70(1+z) E_{1,54}^{-7/134} E_{4,51}^{37/67} \Delta_{1,0,12}^{7/134} \Delta_{4,0,10}^{-1/67} \epsilon_{B,-1}^{6/67} \epsilon_{e,-0.5}^{-160/67} \gamma_{1,1.5}^{-6/67} \zeta_{1/6}^{-6/67} \text{ s}$, the corresponding emission after this time is then

$$f_{\nu,2,p} \simeq$$

$$\left\{ \begin{array}{ll} 2.9 \times 10^7 (1+z) D_{28}^{-2} E_{1,54}^{-1} E_{4,51} \epsilon_{e,-0.5} \gamma_{1,1.5} \gamma_{4,3}^2 \nu_{18}^2 \zeta_{1/6} t_{\oplus,2}^2 \text{ Jy}, & \nu < \nu_{m,2,p} < \nu_{a,2,p} < \nu_{c,2,p}, \\ 7.1 \times 10^9 (1+z)^{\frac{3}{4}} D_{28}^{-2} E_{4,51}^{-\frac{1}{4}} \epsilon_{B,-1}^{-\frac{1}{4}} \gamma_{1,1.5}^{\frac{9}{2}} \gamma_{4,3}^{-\frac{1}{2}} \nu_{18}^{\frac{5}{2}} t_{\oplus,2}^{\frac{11}{4}} \text{ Jy}, & \nu_{m,2,p} < \nu < \nu_{a,2,p} < \nu_{c,2,p}, \\ 4.4 \times 10^{-1} (1+z)^{\frac{14}{5}} D_{28}^{-2} E_{1,54}^{-\frac{7}{10}} E_{4,51}^{\frac{5}{2}} \epsilon_{B,-1}^{\frac{4}{5}} \epsilon_{e,-0.5}^{\frac{6}{5}} \gamma_{1,1.5}^{-\frac{31}{5}} \gamma_{4,3}^3 \nu_{18}^{-\frac{3}{5}} \zeta_{1/6}^{\frac{6}{5}} t_{\oplus,2}^{-\frac{12}{5}} \text{ Jy}, & \nu_{m,2,p} < \nu_{a,2,p} < \nu < \nu_{c,2,p}, \\ 1.7 \times 10^{-2} (1+z)^{\frac{21}{20}} D_{28}^{-2} E_{1,54}^{-\frac{7}{10}} E_{4,51}^{\frac{7}{4}} \epsilon_{B,-1}^{\frac{1}{20}} \epsilon_{e,-0.5}^{\frac{6}{5}} \gamma_{1,1.5}^{-\frac{27}{10}} \gamma_{4,3}^{\frac{7}{2}} \nu_{18}^{-\frac{11}{10}} \zeta_{1/6}^{\frac{6}{5}} t_{\oplus,2}^{-\frac{23}{20}} \text{ Jy}, & \nu_{m,2,p} < \nu_{a,2,p} < \nu_{c,2,p} < \nu. \end{array} \right. \quad (26)$$

The flux density of the reverse shock emission in the case of $\nu_{a,3,p} < \nu_{c,3,p} < \nu_{m,3,p}$ is given by

$$f_{\nu,3,p} \simeq \left\{ \begin{array}{ll} 3.5 \times 10^8 (1+z)^{-1} D_{28}^{-2} E_{4,51}^{-1} \epsilon_{B,-1}^{-1} \gamma_{1,1.5}^8 \nu_{18}^2 t_{\oplus,2}^4 \text{ Jy}, & \nu < \nu_{a,3,p} < \nu_{c,3,p} < \nu_{m,3,p}, \\ 5.3 (1+z)^{\frac{11}{3}} D_{28}^{-2} E_{4,51}^2 \epsilon_{B,-1} \gamma_{1,1.5}^{-\frac{16}{3}} \gamma_{4,3}^{-\frac{1}{3}} \nu_{18}^{\frac{1}{3}} t_{\oplus,2}^{-\frac{7}{3}} \text{ Jy}, & \nu_{a,3,p} < \nu < \nu_{c,3,p} < \nu_{m,3,p}, \\ 2.3 \times 10^{-2} (1+z)^{\frac{3}{4}} D_{28}^{-2} E_{4,51}^{\frac{3}{4}} \epsilon_{B,-1}^{-\frac{1}{4}} \gamma_{1,1.5}^{\frac{1}{2}} \gamma_{4,3}^{\frac{1}{2}} \nu_{18}^{-\frac{1}{2}} t_{\oplus,2}^{-\frac{1}{4}} \text{ Jy}, & \nu_{a,3,p} < \nu_{c,3,p} < \nu < \nu_{m,3,p}, \\ 8.9 \times 10^{-3} (1+z)^{\frac{21}{20}} D_{28}^{-2} E_{4,51}^{\frac{21}{20}} \epsilon_{B,-1}^{\frac{1}{20}} \epsilon_{e,-0.5}^{\frac{6}{5}} \gamma_{1,1.5}^{-\frac{5}{2}} \gamma_{4,3}^{\frac{23}{10}} \nu_{18}^{-\frac{11}{10}} \zeta_{1/6}^{\frac{6}{5}} t_{\oplus,2}^{-\frac{23}{20}} \text{ Jy}, & \nu_{a,3,p} < \nu_{c,3,p} < \nu_{m,3,p} < \nu. \end{array} \right. \quad (27)$$

At time $t_{\oplus} \simeq 3.4 \times 10^2 (1+z) E_{4,51}^{1/2} \epsilon_{B,-1}^{1/2} \epsilon_{e,-0.5}^{1/2} \gamma_{1,1.5}^{-19/8} \gamma_{4,3}^{1/2} \zeta_{1/6}^{1/2} \text{ s}$, $\nu_{c,3,p} = \nu_{m,3,p}$. After that time, the order of the break frequencies becomes $\nu_{a,3,p} < \nu_{m,3,p} < \nu_{c,3,p}$. In this case, the flux density becomes

$$f_{\nu,3,p} \simeq \left\{ \begin{array}{ll} 3.4 \times 10^9 (1+z) D_{28}^{-2} \epsilon_{e,-0.5} \gamma_{1,1.5}^2 \gamma_{4,3} \zeta_{1/6} \nu_{18}^2 t_{\oplus,2}^2 \text{ Jy}, & \nu < \nu_{a,3,p} < \nu_{c,3,p} < \nu_{m,3,p}, \\ 1.0 (1+z)^{\frac{7}{3}} D_{28}^{-2} E_{4,51}^{\frac{4}{3}} \epsilon_{B,-1}^{\frac{1}{3}} \epsilon_{e,-0.5}^{-\frac{2}{3}} \gamma_{1,1.5}^{-\frac{4}{3}} \gamma_{4,3}^{-1} \zeta_{1/6}^{-\frac{2}{3}} \nu_{18}^{\frac{1}{3}} t_{\oplus,2}^{-1} \text{ Jy}, & \nu_{a,3,p} < \nu < \nu_{c,3,p} < \nu_{m,3,p}, \\ 2.3 \times 10^{-1} (1+z)^{\frac{14}{5}} D_{28}^{-2} E_{4,51}^{\frac{9}{5}} \epsilon_{B,-1}^{\frac{4}{5}} \epsilon_{e,-0.5}^{\frac{6}{5}} \gamma_{1,1.5}^{-6} \gamma_{4,3}^{\frac{9}{5}} \zeta_{1/6}^{\frac{6}{5}} \nu_{18}^{-\frac{3}{5}} t_{\oplus,2}^{-\frac{12}{5}} \text{ Jy}, & \nu_{a,3,p} < \nu_{c,3,p} < \nu < \nu_{m,3,p}, \\ 8.9 \times 10^{-3} (1+z)^{\frac{21}{20}} D_{28}^{-2} E_{4,51}^{\frac{21}{20}} \epsilon_{B,-1}^{\frac{1}{20}} \epsilon_{e,-0.5}^{\frac{6}{5}} \gamma_{1,1.5}^{-\frac{5}{2}} \gamma_{4,3}^{\frac{23}{10}} \nu_{18}^{-\frac{11}{10}} \zeta_{1/6}^{\frac{6}{5}} t_{\oplus,2}^{-\frac{23}{20}} \text{ Jy}, & \nu_{a,3,p} < \nu_{c,3,p} < \nu_{m,3,p} < \nu. \end{array} \right. \quad (28)$$

From equations (27) and (28), we can see that the flux densities are the same for the case in which the observed frequency exceeds the three break frequencies.

We consider that many shells like the foregoing shell 4 collide with shell 1 at different radii r_{int} , where r_{int} indicates the observed time by the relation $t_{\oplus} \simeq (1+z)r/(2\gamma_3^2 c)$. Thus the peaks of emission obey a power law temporal profile. Under more realistic conditions, “shell 1” may be sole, proceeding at the front, and many shells like “shell 4” ejected from the central engine continually overtake “shell 1” (see Figure 1). As the energy of “shell 1” is assumed to be much greater than that of “shell 4”, the dynamics of “shell 1” after the collision can be almost unchanged, and thus the above relations are still applicable. In the popular collapsar model, “shell 1” can be understood as due to the envelope of a collapsing massive star. Because a relativistic outflow needs to accumulate enough energy to break out of the envelope and is inevitably polluted by the baryons in the envelope, this outflow (i.e., “shell 1”) should be more energetic but have less Lorentz factor comparing with “shell 4”.

3. GRB 050904

Using the above model, we fit the peaks of the X-ray light curves of GRB 050904 in the observer’s frame. We consider the model parameters $E_1 = 10^{55}$ erg, $E_4 = 1.1 \times 10^{51}$ erg, $\gamma_1 = 31.6$, $\gamma_4 = 1455$, $\Delta_{1,0} = 10^{12}$ cm, $\Delta_{4,0} = 2.0 \times 10^8$ cm, $\epsilon_B = 0.1$, $\epsilon_e = 0.316$, and $p = 2.2$ and the cosmology with $\Omega_m = 0.23$, $\Omega_\lambda = 0.73$ and $H_0 = 71 \text{ km s}^{-1} \text{ Mpc}^{-1}$. These parameters lead to a Newtonian forward shock and a relativistic reverse shock. As shown in Figure 2, the solid line with four segments is fitted analytically. The flux is an integral of flux density in a frequency range of 4×10^{16} Hz to 2×10^{18} Hz, which corresponds to XRT’s 0.2-10 keV band. The temporal breaks are due to crossing of the three break frequencies.

The first segment represents the emission from a relativistic reverse shock with a constant shell width, which satisfies equation (13) with temporal index 1/2. At time ~ 42 s, the corresponding radius is $R(42 \text{ s}) \simeq 2\gamma_3^2 ct_\oplus / (1+z) \simeq 3.5 \times 10^{14}$ cm, while the spreading radii of region 1 and region 4 are $R_{s,1} \simeq \gamma_1^2 \Delta_{1,0} \simeq 10^{15}$ cm, and $R_{s,4} \simeq 4.2 \times 10^{14}$ cm respectively. The three radii are approximately equal, and thus $R(42 \text{ s})$ can be taken as the common spreading radius of regions 1 and 4.

After the first break time, regions 1 and 4 should be spreading and the flux density is described by the third expression of equation (27). The temporal index is $-1/4$. Up to ~ 350 s, the frequency $\nu_{m,3,p} \simeq 2.6 \times 10^{17}$ Hz decreases to the observed frequencies of XRT, and then the order of the break frequencies becomes $\nu_{a,3,p} < \nu_{c,3,p} < \nu_{m,3,p} < \nu$ or $\nu_{a,3,p} < \nu_{m,3,p} < \nu_{c,3,p} < \nu$. The flux density is given by the last expression of equation (27), and the temporal index of flux is $-23/20$. After $\sim 3 \times 10^4$ s, the order is $\nu_{a,3,p} < \nu_{m,3,p} < \nu < \nu_{c,3,p}$, and the temporal index becomes $-12/5$.

Observationally it was reported that the photon indices are ~ -1.3 and ~ -1.9 (whose corresponding spectral indices are -0.3 and -0.9 respectively) at early and late times respectively (Cummings et al. 2005; Watson et al. 2005). The observer’s time at which the spectral index changed is about 350 s. This time can be naturally understood as the crossing time of ν_m to ν . Before this crossing time, $\nu_c < \nu < \nu_m$ and the spectral index is $-1/2$, and after this crossing time, $\nu_c < \nu_m < \nu$ and the index is -1.1 . Figure 3 shows the spectral index evolution and a sketch for the evolution of spectral energy distribution. These spectral indices are generally slightly less than the observed ones, because our model only gives the spectral indices at the peak times but the observations were performed in relatively broad ranges of time. At the beginning of each pair of reverse and forward shocks, the cooling frequency ν_c is very large (Zou, Wu & Dai 2005), because this frequency is proportional to t_{co}^{-2} , where t_{co} is the comoving time of the shocks. Thus ν_c can be larger than ν during the initial stage of the shocks. In the case of $\nu < (\nu_m, \nu_c)$, the spectral index is 1/3, which makes the observed spectral index larger than the expected values -0.5 and -1.1 .

The optical data during the same period were reported (Haislip et al. 2005; Boër et al. 2005). The observed J-band (2.47×10^{14} Hz) data are plotted in Figure 2 in units of magnitude. Using the above parameters, we plot a line representing the J-band peak flux density. However, the J-band emission may be mainly contributed by the forward shocks. Since the forward shocks are Newtonian, the emission contributes more at optical band than does at the X-ray band. Furthermore, as the number density of the forward-shocked region is much larger than that of the reverse shocks (see equations (14) and (15)), the contribution to the J-band emission exceeds that of the reverse shocks. To show the contribution of the forward shocks, Figure 4 duplicates Figure 2 but counts in the forward shocks. It is reasonable to see that the fitted peaks are greater than the observed data. As the fitting lines stand for the peak fluxes of the emission of internal shocks, these fluxes should be greater than the time-averaged observed data especially for the optical emission, which lasts a relatively longer time for the observation. If there are not reverse-forward shocks at a certain time, the observed flux density should be much less than the expected peak one. Therefore, the fitting solid line is basically consistent with the observed data.

For the highest (fourth) J-band point (449s-589s) and the X-ray peak nearly at the same time, we suggest that they could arise from the same internal shocks, and the X-ray peak could occur only at time slightly earlier than ~ 440 s (we circled them in Figure 4 for emphasis). There is a time lag ($\sim 0 - 140$ s) between the X-ray emission and the J-band emission. This may be caused by a spectral time lag (Norris, Marani & Bonnell 2000), the different refractivities of photons in different energy bands during the propagation from the source to the earth, or a quantum gravity effect (which is also due to different refractivities in vacuum for different photons, Amelino-Camelia et al. (1998)). There has also been an example with a long time lag, GRB 980425 (Norris, Marani & Bonnell 2000), which shows the probability of time lag with tens of seconds.

We further show that our model is consistent with the observed data at some other aspects. Firstly, the Lorentz factor of region 1 should not change significantly during the period of X-ray emission. Because faster ejected shells (region 4) have much less kinetic energy than the front slower one (region 1) and the forward shocks are Newtonian, the Lorentz factor and the particle number of region 1 do not increase significantly when it is overtaken by faster shells. On the other hand, we estimate the deceleration radius $r_d \equiv [3E_0/(4\pi\gamma^2nm_p c^2)]^{1/3}$, where E_0 is the isotropic-equivalent kinetic energy, and n is the medium density. Letting the gamma-ray isotropic equivalent energy be $E_{\gamma,iso} = 2.5 \times 10^{54}$ erg, which is consistent with the observation range (Cusumano et al. 2005), and assuming the radiative efficiency $\eta = 0.2$ and the medium density $n = 3.16\text{cm}^{-3}$, we obtain $E_0 = E_{\gamma,iso}(1 - \eta)/\eta = 1 \times 10^{55}$ erg. This energy is consistent with the parameters assumed above. And then the deceleration radius is $r_d \simeq 8.0 \times 10^{17} E_{0,55}^{1/3} \gamma_{1.5}^{-2/3} n_{0.5}^{-1/3}$ cm, which corresponds to the observed time

$t_{\oplus} \simeq 9.7 \times 10^4 [(1+z)/7.29] E_{0.55}^{1/3} \gamma_{1.5}^{-8/3} n_{0.5}^{-1/3}$ s. This deceleration time is larger than the X-ray duration time, indicating that region 1 is not decelerated by the ambient medium during this period.

Secondly, the Lorentz factor at the jet-break time (Tagliaferri et al. 2005) is about $1/\theta_j \simeq 17.5$ ($\theta_j \simeq 0.057$). It should be greater at an earlier time. This is in agreement with our used parameter ($\gamma_1 = 31.6$).

Thirdly, we note the photon indices at the second break of the fitting X-ray peak line in Figure 2. The indices are -1.22 ± 0.10 during the time period of (149s, 223s), -1.5 ± 0.3 during the time period of (223s, 303s) in the BAT data, and -1.13 ± 0.07 during the time period of (169s, 209s), -1.31 ± 0.06 during the time period of (209s, 269s), -1.34 ± 0.06 during the time period of (269s, 371s) in the XRT data (Table 1 of Cusumano et al. 2005, where the time is divided by $(1+z)$ to give the local observer’s frame). It can be seen that the photon indices of the BAT data are greater than those of the XRT data. In our model, the frequency ν_m is crossing the observed frequency during this period. For the frequency orders $\nu_c < \nu < \nu_m$ and $\nu_c < \nu_m < \nu$, the flux densities are scaled as $f_{\nu} \propto \nu^{-1/2}$ and $f_{\nu} \propto \nu^{-11/10}$ respectively. Therefore, the spectrum is harder for the lower-frequency emission than for the higher-frequency emission, which is consistent with the observed data.

Fourthly, the mean intrinsic column density is $N_H = (2.30 \pm 0.50) \times 10^{22} \text{cm}^{-2}$, as measured by XRT (Cusumano et al. 2005). This high density cannot be explained by the ambient medium with assumed number density 3cm^{-3} . Because the radiation originates from the reverse-forward shocks and should pass through “shell 1”, we find that the column density of “shell 1” is $N_H = E_1 / (\gamma_1 4\pi r^2 m_p c^2)$, which is $1.67 \times 10^{23} \text{cm}^{-2}$ at radius $r = 10^{16} \text{cm}$ and $1.67 \times 10^{21} \text{cm}^{-2}$ at radius $r = 10^{17} \text{cm}$. These values are basically consistent with the measured mean column density. Therefore, the materials in “shell 1” provide an explanation for the high column density measured by XRT.

Finally, there are several low peaks in figure 2 at about 10^3s . They may be caused by non-uniform Lorentz factors or energies of the ejected rapid shells.

In short, the X-ray flares are understood as due to the internal shocks. These shocks are caused by the continually ejected faster shells that overtake the sole slower one with much larger kinetic energy and much more baryons.

4. Conclusions and discussion

In this paper, we have proposed a simple internal shock model: a slower massive shell propagates in the front, and many faster shells with similar mass and energy catch up with the front slower shell at different radii. These collisions lead to reverse-forward shocks. The shocks produce the γ -ray and lower-energy emission by synchrotron radiation. We obtained a “normal” set of parameters to fit the peak fluxes of XRFs of GRB 050904, and found that our model is well consistent with the observations including the early optical data.

For GRB 050904, we also found that the contribution of the forward shock emission is insignificant in the X-ray band, but significant in the J-band at early times, because the frequency of emission from the Newtonian forward shocks mainly lies in the optical band. However, we should note that, for other bursts, forward shocks may also be important for the X-ray emission. If the leading shell (“shell 1”) is not more energetic than the followed faster shells (“shells 4”), the velocity of “shell 1” cannot be regarded as unchanged after some collisions and the simple model in section 2 is invalid. If the parameters differ, the deceleration radius may be smaller, and the external shock may become important. All the effects would change the profile of the XRF peaks.

In general, we argued that some long bursts should have the same properties: the peaks are nearly constant before the time at which ν_m is just equal to the observed frequency ν , and decline rapidly with temporal index about $-(3p - 2)/4$ after this time. Therefore, the γ -ray emission of these bursts persists up to the time when $\nu_m = \nu$, and disappears because of the rapid decline. In this case, the γ -ray emission ceases when the peak energy $E_p \simeq h\nu$. There are two other reasons for the disappearance of γ -rays. One is that the flux of γ -ray emission decreases below the detectable limits of telescopes when the frequency order is still $\nu_c < \nu < \nu_m$. The other is the turnoff of the central engine when ν_m is still larger than ν . Only in the latter case, it can be said that the γ -rays duration is the burst duration.

We would like to thank the referees for valuable comments that have allowed us to improve our manuscript and X. F. Wu, L. Shao, Y. F. Huang, B. Zhang and Y. Z. Fan for helpful discussions. The formulae were generated by the help of Maxima. This work was supported by the National Natural Science Foundation of China (grants 10233010 and 10221001).

REFERENCES

- Amelino-Camelia G., Ellis J., Mavromatos N. E., Nanopoulos D. V., & Sarkar S., 1998, *Nature*, 393, 763
- Blandford R. D., & McKee C. F. 1976, *Phys. Fluids*, 19, 1130
- Boër M., et al. 2006, *ApJ*, 638, L71
- Burrows D. N., et al. 2005, *Science*, 309, 1833
- Cummings J., et al. 2005, *GCN*, 3910
- Cusumano G., et al. 2005, *Nature*, 440, 164
- Dai, Z. G., Wang, X. Y., Wu, X. F. & Zhang, B. 2006, *Science*, 311, 1127
- Faber, J. A., Baumgarte, T. W., Shapiro, S. L., & Taniguchi, K. 2006, *ApJ*, submitted, astro-ph/0603277
- Fan Y. Z., & Wei D. M. 2005, *MNRAS*, 364, L42
- Haislip J. B., et al. 2005, *Nature*, 440, 181
- Kawai N., Yamada T., Kosugi G., Hattori T. and Aoki K. 2005, *GCN*, 3937
- Mászáros P., & Rees M. J. 1993, *ApJ*, 405, 278
- Mászáros P., & Rees M. J. 1999, *ApJ*, 306, L39
- Norris, J. P., Marani G. F., & Bonnell J. T., 2000, *ApJ*, 534, 248
- Nousek J. A. et al. 2006, *ApJ* accepted (astro-ph/0508332)
- O’Brien P. T. et al. 2006, *ApJ* submitted (astro-ph/0601125)
- Perna, R., Armitage, P.J., & Zhang, B., 2006, *ApJ*, 636, L29
- Piran T., Shemi A., & Narayan R. 1993, *MNRAS*, 263, 861
- Price P. A., Cowie L. L., Minezaki T., Schmidt B. P., Songaila A., & Yoshii Y. 2005, *ApJL*, submitted (astro-ph/0509697)
- Proga, D., & Zhang, B., 2006, *MNRAS*, submitted, astro-ph/0601272
- Rees M. J., & Mészáros P. 1994, *ApJ*, 430, L93

Sari R., & Piran T. 1995, ApJ, 455, L143

Tagliaferri G., et al. 2005, A&A, 443, L1

Watson D., et al. 2006, ApJ, 637, L69

Wei D., Yan T., & Fan Y. Z., 2005, ApJ, 636, L69

Wu X. F., Dai Z. G., Huang Y. F., & Lu T. 2003, MNRAS, 342, 1131

Wu X. F., et al., 2005, preprint(astro-ph/0512555)

Zhang B., et al. 2005, ApJ accepted (astro-ph/0508321)

Zou Y. C., Wu X. F., & Dai Z. G. 2005, MNRAS, 363, 93

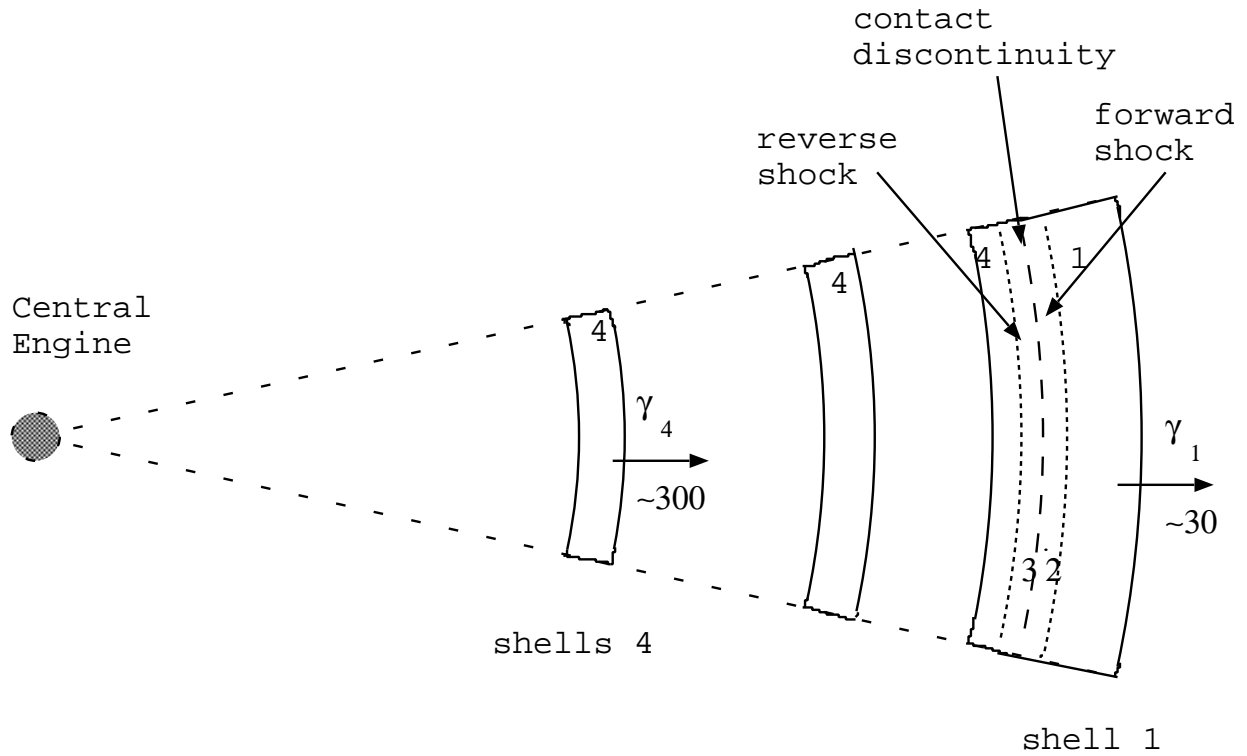


Fig. 1.— Sketch of our model: A slower shell labeled “1” with much more energy expands in the front. Many similar faster shells labeled “4” with less energy and less number density catch up with “shell 1”, and reverse-forward shocks occur. The gamma rays and early X-rays are mainly emitted from the reverse shocks.

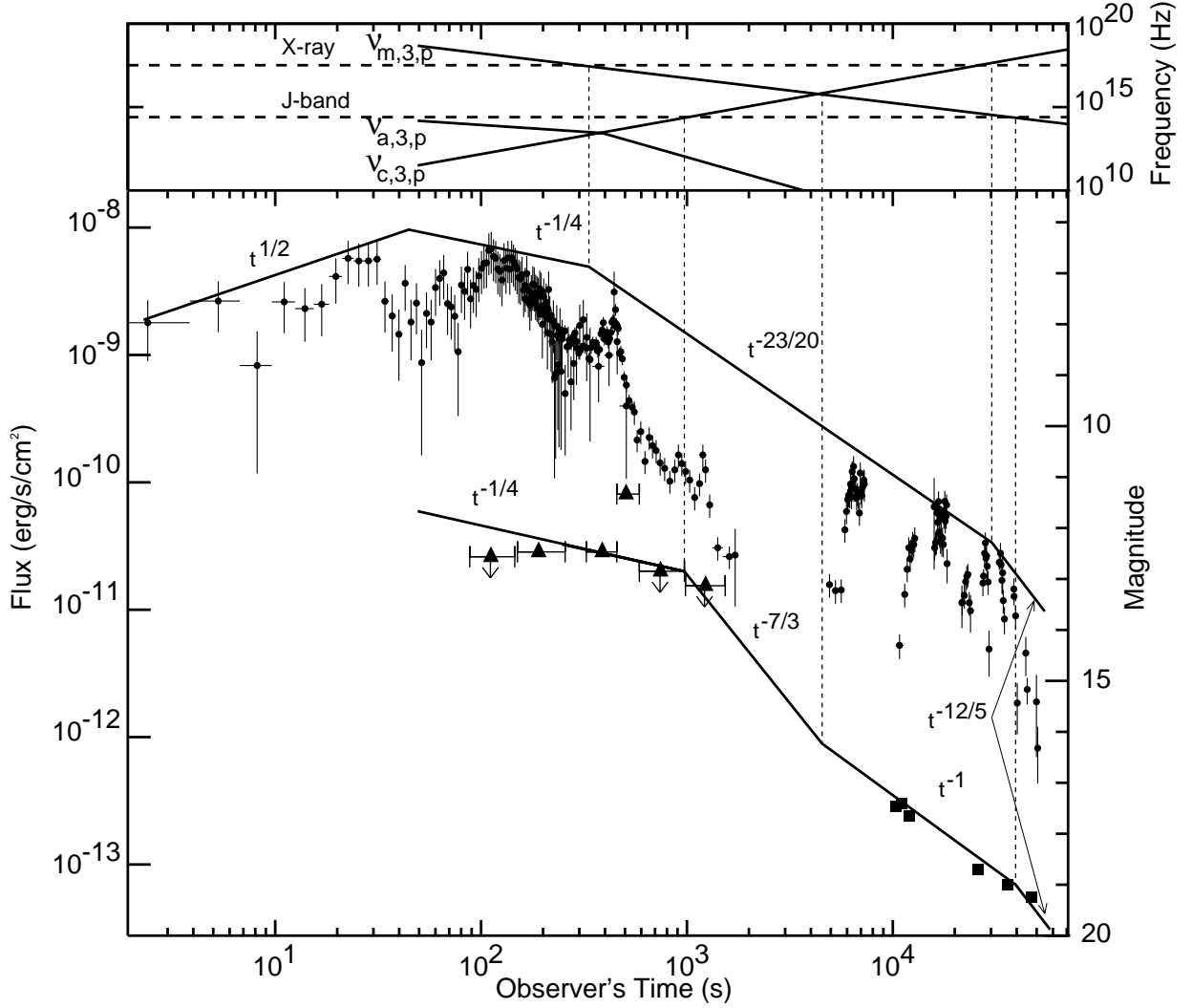


Fig. 2.— Fitting to the peaks of X-ray and optical light curves of GRB 050904 (solid line). The observed X-ray data (points with error bars) are taken from Cusumano et al. (2005) where the flux is divided by $(1+z)^2$ and the time is multiplied by $(1+z)$ to give the observer’s frame. The optical data are taken from Boër et al. (2005) (triangles with error bars, extrapolated to J-band by the relation $F_\nu \propto \nu^{1/3}$, which is the synchrotron emission in the case $\nu_a < \nu < \nu_c < \nu_m$) and Haislip et al. (2005) (squares). The top panel shows the break frequencies as functions of time. Vertical dashed lines represent the crossing times of any two frequencies.

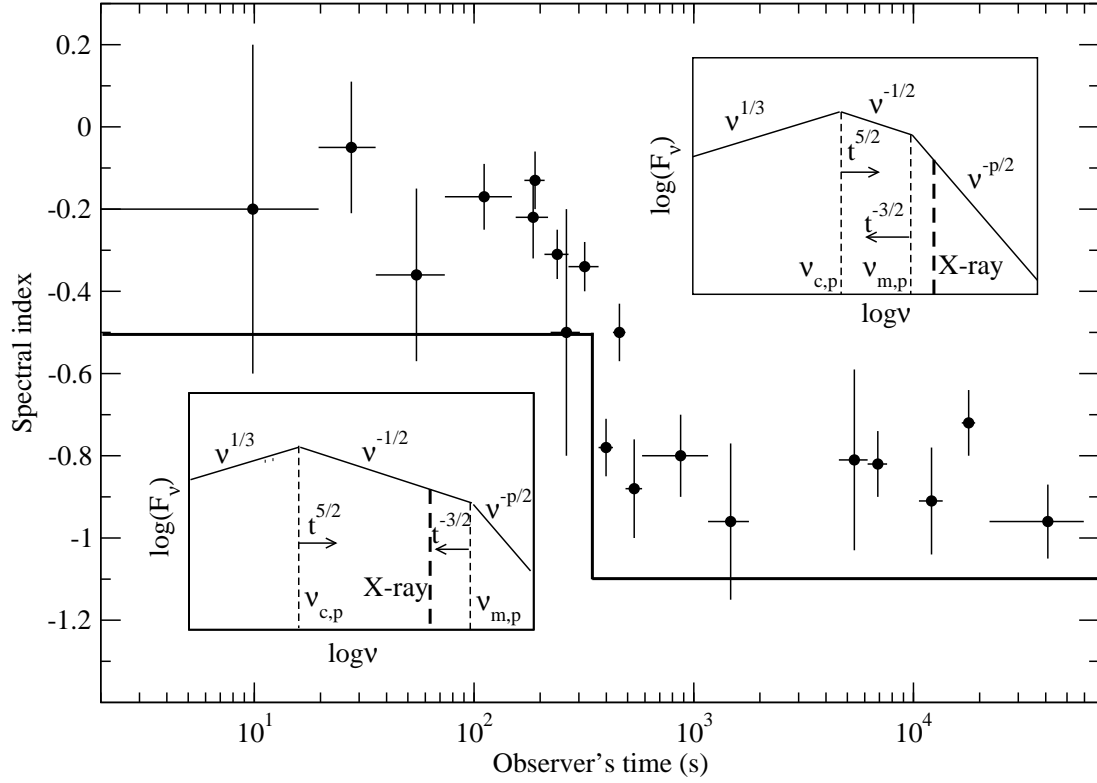


Fig. 3.— Spectral index evolution. The thick solid line is the expected spectral index at the peak of synchrotron radiation. The corresponding spectral energy distribution for the two index values (-0.5 and -1.1) are plotted schematically in the two sub-figures. The points with error bars are taken from Cusumano et al. (2005).

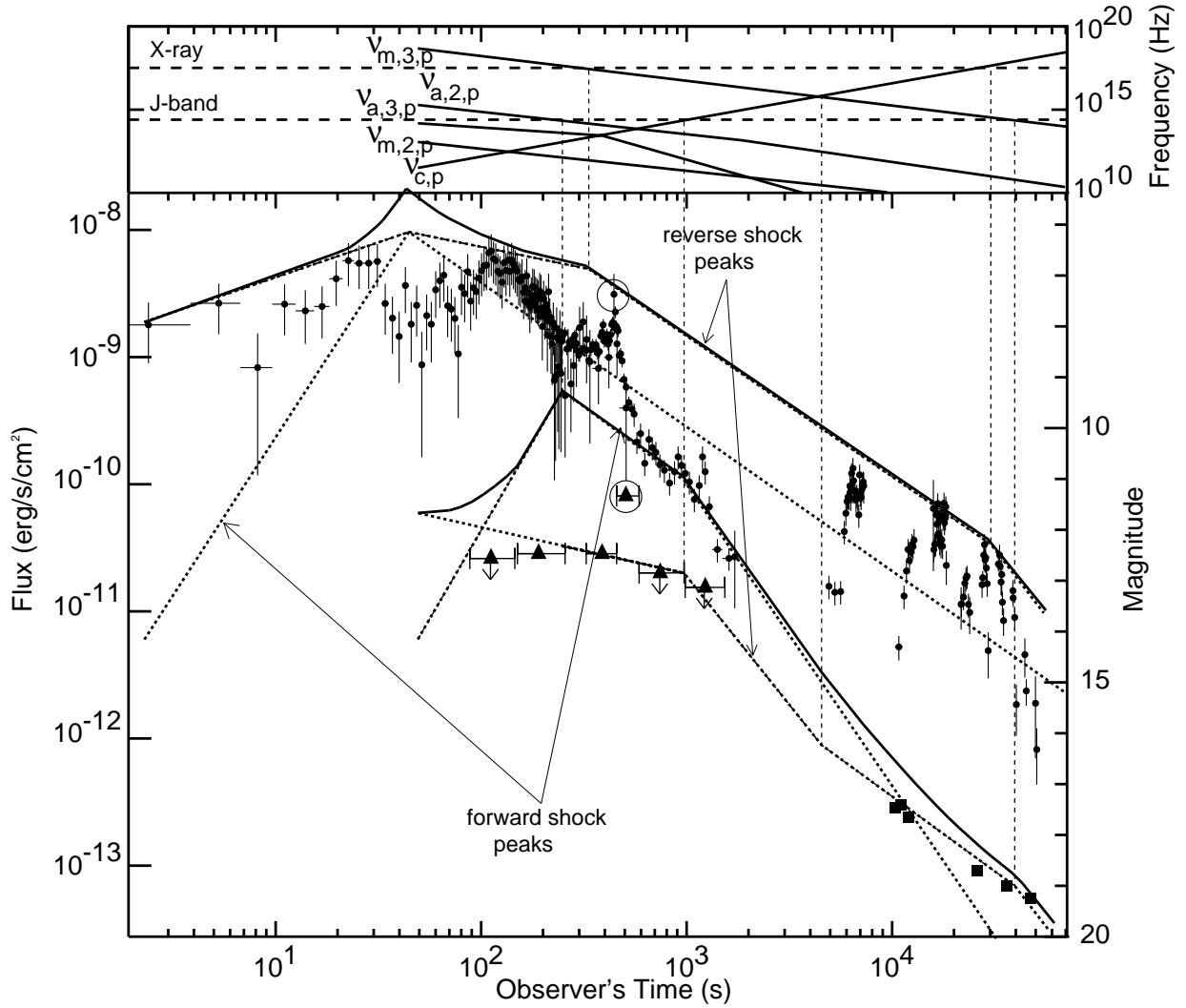


Fig. 4.— Same as Figure 2 except for counting in the contribution of the forward shocks. The solid line indicates the total peak flux density and the others are annotated in this figure.